Transonic Aeroelastic Calculation with Full Implicit Subiteration and Deforming Grid Approach

Guowei YANG[1] and Shigeru OBAYASHI[2]

ABSTRACT

Through the coupling of subiteration between aerodynamic and structural governing equations, a full implicit finite-volume aeroelastic solver has been developed for transonic flutter simulation. The subiteration algorithm of the Navier-Stokes fluid equations is constructed based on the LU-SGS scheme and the subiteration formulation is applied directly to the structural equations of motion in generalized coordinates. In the flutter calculation, a modified grid deformation approach that maintains the grid quality even under large deflections and rotations has been applied. Results are presented for the AGARD 445.6 standard aeroelastic wing configuration over subsonic to supersonic Mach number range. Predictions of flutter points are compared with experimental data and with simulations previously reported. The effects of grid resolution and time-step sizes are also investigated.

1. Introduction

In recent years, dynamic aeroelastic simulations by solving three-dimensional Navier-Stokes equations coupled with structural equations of motion have been extensively studied [1-3]. However, in these methods, the flow governing equations are only loosely coupled with structural equations, namely, after the aerodynamic loads are determined by solving the flow governing equations, the structural model is used to update the position of body. The coupling contains the error of one time step, thus these methods are always only first-order accuracy in time regardless of the temporal accuracy of the individual solvers of the flow and structural equations. In addition, due to the deformation of aeroelastic configuration, adaptive dynamic grids need to be generated at each time step. In the existing aeroelastic methods, various adaptive algebraic grid-generation methods were applied for their applications.

A recently developed method by Melville et al [4], which uses an implicit scheme for the flow and structural equations, achieves a full implicit coupling between the fluids and structures via subiterations. The flow solver in this scheme is the three-dimensional Beam-Warming algorithm. A grid deformation approach was also developed for aeroelastic application, which maintains the grid quality of the initial mesh near deforming surface under moderate deflections and rotations.

The aeroelastic applications mentioned are all based on finite difference schemes. In the paper, a cell-center finite volume code is implemented for the aeroelastic calculation. The LU-SGS subiteration algorithm is constructed for the thin-layer Navier-Stokes equations, and the modified Harten-Lax-van Leer Einfeldt (HLLE) scheme by Obayashi et al [5] is used for the discretization of convective terms of the flow governing equations. The structural equations of motion in generalized coordinates are employed for the calculation of structures. Modified grid deformation approach suitable for the large aeroelastic deformation is also developed.

The AGARD445.6 standard aeroelastic wing test case [6] is applied to validate the resulting aeroelastic solver. Two cases with Mach numbers 0.96 and 1.141 are computed and compared with experimental data, as well with other computations. Predicted flutter boundary is compared with the experimental values over the Mach number range 0.338-1.141. The effects of grid resolution, time-step sizes are investigated. The computational efficiency of the full implicit method is evaluated by

1. Guest Researcher, Institute of Fluid Science, Tohoku University.
2. Associate Professor, Institute of Fluid Science, Tohoku University.

comparison with the loosely coupling method.

2. Governing Equations

Aerodynamic Governing Equations

Aerodynamic governing equations are the unsteady, three-dimensional thin-layer Navier-Stokes equations in strong conservation law form, which can be written in curvilinear coordinates as

$$\partial_t \hat{Q} + \partial_\xi F + \partial_\eta G + \partial_\zeta H = \partial_\zeta H_v + S_{GCL} \qquad (1)$$

In the formulation, all variables are normalized by the appropriate combination of freestream density, freestream velocity and wing root chord length. The viscosity coefficient μ in H_v is computed as the sum of laminar and turbulent viscosity coefficients, which are evaluated by the Sutherland's law and Baldwin-Lomax model[7]. The source term S_{GCL} is obtained from the geometric conservation law [8] for moving mesh, which is defined as

$$S_{GCL} = Q\left[\partial_t J^{-1} + (\xi_t / J)_\xi + (\eta_t / J)_\eta + (\zeta_t / J)_\zeta\right] \qquad (2)$$

The term vanishes automatically for the common unsteady flow simulation that the grid is only rotated and translated with a rigid motion at each time step.

Structural dynamic Governing Equations

Second-order linear structural dynamic governing equations after normalized similar to the flow governing equation can be written as

$$[M]\{\ddot{d}\} + [K]\{d\} = \{F\} \qquad (3)$$

$[M]$ and $[K]$ are the non-dimensional mass and stiffness matrices, respectively. $\{F\}$ and $\{d\}$ are the aerodynamic load and displacement vectors, respectively. In order to solve Equation 3, the Rayleigh-Ritz method is used and the deduced structural equation in generalized coordinates is

$$\ddot{q}_i + 2\zeta_i \omega_i \dot{q}_i + \omega_i^2 q_i = [\Phi]_i^T F / M_i \qquad (4)$$

where

$$\{d\} = [\Phi]\{q\}, \quad \omega_i^2 = [\Phi]_i^T [K][\Phi], \quad M_i = [\Phi]_i^T [M][\Phi]$$

The modal damping is readily added on the left hand side of Equation 4, where ζ_i is the damping ratio in the i th mode. The equation can be written as a first-order system by defining $S = [q, \dot{q}]$:

$$\dot{S} + \begin{bmatrix} 0 & -1 \\ \omega_i^2 & 2\omega_i\zeta_i \end{bmatrix} S = \begin{bmatrix} 0 \\ [\Phi]_i^T F / M_i \end{bmatrix} \qquad (5)$$

3. Numerical Method

LU-SGS method of Yoon and Jameson [8], employing a Newton-like subiteration, is used for solving Equation 1. Second-order temporal accuracy is obtained by utilizing three-point backward difference in the subiteration procedure. The numerical algorithm can be deduced as

$$\begin{aligned} & LD^{-1}U\Delta Q \\ & = -\phi^i \{(1+\phi)Q^p - (1+2\phi)Q^n + \phi Q^{n-1} \\ & - J\Delta t Q^p \left[(\xi_t / J)_\xi + (\eta_t / J)_\eta + (\zeta_t / J)_\zeta\right]^p \\ & + J\Delta t(\delta_\xi F^p + \delta_\eta G^p + \delta_\zeta (H^p - H_v^p))\} \end{aligned} \qquad (6)$$

where

$$L = \overline{\rho} I + \phi^i J\Delta t(A^+_{i-1,j,k} + B^+_{i,j-1,k} + C^+_{i,j,k-1})$$

$$D = \overline{\rho} I$$

$$U = \overline{\rho} I - \phi^i J\Delta t(A^-_{i+1,j,k} + B^-_{i,j+1,k} + C^-_{i,j,k+1})$$

and

$$\overline{\rho} = 1 + \phi^i J\Delta t(\overline{\rho}(A) + \overline{\rho}(B) + \overline{\rho}(C))$$

$$\phi^i = 1/(1+\phi) \quad , \quad \Delta Q = Q^{p+1} - Q^p$$

Here $\phi = 0.5$ and Q^p is the subiteration approximation to Q^{n+1} . The deduced subiteration scheme reverts to the standard first-order LU-SGS scheme for $\phi = 0$ and $p = 1$.

The inviscid terms in Equation 6 are approximated by modified third-order upwind HLLE scheme of Obayashi et al [5]. For the isentropic flow, the scheme results in the standard upwind-biased flux-difference splitting scheme of Roe, and as the jump in entropy becomes large in the flow, the scheme turns into the standard HLLE scheme. Thin-layer viscous term is discretized by second-order central difference.

The subiteration method can also be applied to the structural equations of motion in generalized coordinates

of Equation 6. The resulting scheme is

$$\begin{bmatrix} 1 & -\phi^i \Delta t \\ \phi^i \Delta t \omega_i^2 & 1+2\phi^i \omega_i \zeta_i \Delta t \end{bmatrix} \Delta S$$
$$= -\phi^i \{(1+\phi) S^p - (1+2\phi) S^n + \phi S^{n-1} \qquad (7)$$
$$+ \Delta t \begin{bmatrix} 0 & -1 \\ \omega_i^2 & 2\omega_i \zeta_i \end{bmatrix} S^p - \Delta t \begin{bmatrix} 0 \\ [\Phi]_i^T F^p / M_i \end{bmatrix} \}$$

where $\Delta S = S^{p+1} - S^p$.

As $p \to \infty$, a full implicit second-order temporal accuracy scheme for aeroelastic computation is formed by the coupling solutions of Equation 6 and 7. Numerical experiments indicate the calculated results are nearly unchangable as $p \geq 3$. In the following calculation, the number of subiteration is set to 3.

4. Grid Deformation Method

For the aeroelastic application, if the grid is regenerated at every time step, then the elaborate and time-consuming grid-generation method cannot be used. So in most common aeroelastic sovlers, only algebraic grid generation methods are employed. Recently, a grid deformation method was developed for the aeroelastic calculation by Melville et al [9]. The initial grid of high quality can be generated with any elaborate grid-generation method. The adaptive dynamic grid at each time step is obtained by an algebraic grid deformation approach and the grid maintains nearly the same quality of the initial mesh.

First a reference grid $r_{i,j,k}$ is constructed from the initial grid $x_{i,j,k}$ and the deformed surface grid point $x'_{i,j,1}$ calculated from the structural equations.

$$r_{i,j,k} = x_{i,j,1} + \Delta x_{i,j,1} + [R](x_{i,j,k} - x_{i,j,1}) \qquad (8)$$

where $\Delta x_{i,j,1} = x'_{i,j,1} - x_{i,j,1}$ is the deformed size of the surface grid and $[R]$ is the surface rotation matrix defined by unit normal vectors of the original surface and the perturbed surface. The new dynamic grid can be generateded by applying a blending function to the reference grid and the original grid:

$$x'_{i,j,k} = b_{i,j,k} x_{i,j,k} + (1 - b_{i,j,k}) r_{i,j,k} \qquad (9)$$

A blending choice is a cubic function in arclength space with zero slope at the endpoints, which maintains the wall grid orthogonality and grid smoothly transitions in the far field. This can be written as

$$b_{i,j,k} = 3(s_{i,j,k} / s_{i,j,k_{\max}})^2 - 2(s_{i,j,k} / s_{i,j,k_{\max}})^3 \qquad (10)$$

where $k_{\max}$ is the last node in the grid normal direction.

The above grid deformation method is only suitable for moderate aeroelastic deformation. For the larger aeroelastic deformation, because the far field nodes of reference grid would deflect too much comparing with the original grid, the method cannot be used.

The limitation of the above method can be overcome by generating an initial grid at each time step rather than simply using the original grid. For the common unsteady calculation, we usually let the grid rigidly attach to the body and the grid is rotated and translated in a rigid body motion fashion after each time step. First the initial sectional grid is translated and let its leading edge coincide with the leading edge of the deformed section. Then the sectional grid is rotated around the leading edge and let its chord coincide with that of the deformed section. The grid generated with the rigid translation and rotation may correspond to the reference grid determined by Equation 9 at the far field. It is evident that the limitation of the above grid deformation method can be overcome using the rotated and translated grid as an initial grid at each time step.

5. Results and Discussions

The AGARD 445.6 weakened wing model [6] is considered, which has an aspect ratio 1.6525, a taper ratio of 0.6576, a quarter-chord swept angle of 45 deg and a NACA 65A004 airfoil section.

A typical C-H grid is generated by the elaborate elliptic equations, which includes full control of the grid line distance and the orthogonality at the surface boundary. Figure 1 shows the root sectional grid and surface grid of the wing. The far field boundaries of the grid locate at 9 root chord lengths downstream of the trailing edge, 8 root chord lengths to the upper, lower, and upstream surface boundaries, and 4 root chord lengths from wing tip. For the baseline grid of

161×51×43, there are 121 grid points around the wing surface, and 39 grid points on the spanwise direction of wing surface. For the refined grid of 181×51×63, 20 grid points are added both in the chord and normal directions.

The first four structural modes and natural frequencies provided in the reference [6] are used for the present computation. To match the given mode shapes to the corresponding aerodynamic surface grid, linear and spline interpolations are employed in the chord and spanwise directions. Although measured values of structural damping coefficient were not given in reference [6], in general, they were of the order of 0.01. It is set to zero in the whole calculations.

First, flutter analysis are carried out at two Mach numbers, $M_\infty = 0.96$ and $M_\infty = 1.141$. Each Mach number is run for several dynamic pressures to determine the flutter point. As the dynamic pressure is varied, the freestream density and Mach number are held fixed and Reynolds number is allowed to vary. Then flutter boundary and frequency are compared with predicted and experimental values over subsonic to supersonic Mach number range.

A nondimensional time step $\Delta t = 0.05$ is used for the flutter compuations unless stated. All simulations are started from its corresponding steady flow. At $t = 0$, a small initial velocity pertubation 0.0001 for the first bending mode is applied to the wing.

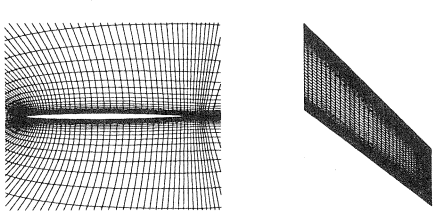

Fig. 1 Root sectional grid and surface grid for the AGARD 445.6 wing

The First Computational Test Case $M_\infty = 0.96$

The response of the first four modes is shown on the left hand of Figure 2 for the $M_\infty = 0.96$ case on the baseline mesh for dynamic pressure $q/q_e = 1.0$, where the experimental dynamic pressure for flutter is $q_e = 61.3$ lbf/ft^2. The dominant mode appears to be the first bending mode, and only second mode has some effects to the first mode. The amplification factor of first bending mode is analyzed, which is defined as the ratio of the magnitude of a peak with the magnitude of the previous peak of the same sign. Its corresponding response frequency is determined from the period between these two peaks. For the present case, the amplification and response frequency calculated from the average of the values for the last positive and negative peaks are $AF = 1.023$, and $\omega = 84.135$ rad/sec. The response of the first four modes for a flutter condition $q/q_e = 1.2$ is shown on the right hand of Fig. 2. Its corresponding amplification factor and frequency is $AF = 1.093$ and $\omega = 89.559$ rad/sec.

Based on the results of the above two calculations, the dynamic pressure and frequency for flutter ($AF = 1.0$) can be interpolated linearly as $q/q_e = 0.934$, $\omega = 82.353$ rad/sec.

The flutter points are compared with other computed results [2-4] and with experimental results [6] in Table 1. where U_f is the flutter speed, b_s is half the root chord, ω_α is the primary torsional frequency, and $\overline{\mu}$ is mass ratio. In reference [4], Gordinier et al computed in detail the case with central difference scheme and the implicit approximately factored finite difference algorithm of Beam and Warming, employing a Newton-like subiteration procedure. Viscous and inviscid results were presented for the grid resolution of three grids. In Table 1, only their viscous computed result for the medium grid is included. Even for their medium grid, its grid number is more than that of the present grid used.

For the baseline grid and the size of time step 0.05, the present computation slightly underpredicts the experimental flutter speed and frequency. But it is much closer to the experimental values than that of other computations. The effect of the size of time step and grid resolution on the response of the first bending mode for $q/q_e = 1$ is demonstrated on the left hand of Fig. 3 and Table 2. There are only small differences between them. To compromise the computational efficiency and accuracy, the choice of time-step size and grid is appropriate for the present case. It is seen the reduction of time-step size leads to slightly reduction of amplification factor and finer grid grows slightly the oscillation. This indicates that the effect of small

time-step size is to reduce the computed flutter speed, but the effect of improved mesh resolution is to increase the speed.

Table 1 Summary of flutter point predictions at $M_\infty = 0.96$

Method	q/q_e	$U_f/(b_s\omega_\alpha\sqrt{\overline{\mu}})$	ω/ω_α
Present	0.934	0.301	0.353
Experiment	1.0	0.308	0.365
Reference 2	1.47	0.367	0.349
Reference 3	0.89	0.294	0.346
Reference 4	1.12	0.329	0.376

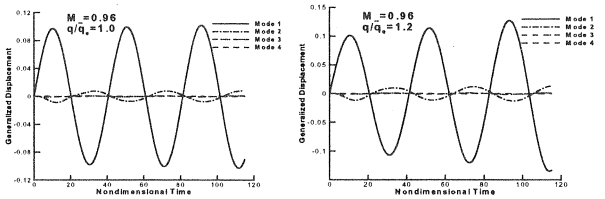

Fig. 2 Dynamic response of first four modes at $M_\infty = 0.96$, $q/q_e = 1.0$ and $q/q_e = 1.2$

Table 2 Effects of grid and time-step sizes, $M_\infty = 0.96, q/q_e = 1.$

Grid	Δt	AF	ω
Baseline	0.05	1.024	84.135
Baseline	0.025	1.008	84.395
Fine	0.05	1.035	83.877

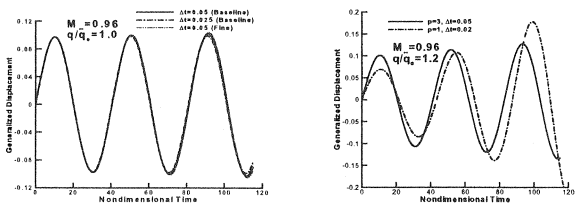

Fig. 3 Effect of grid, time-step sizes and subiterations on mode 1 response at $M_\infty = 0.96$, $q/q_e = 1.0$ and $q/q_e = 1.2$

The computational efficiency of the full implicit method ($p = 3$, $\Delta t = 0.05$) is also evaluated by the comparison with the method in which subiteration is not used ($p = 1$) and structural equations of motion are solved using the standard four-stage Runge-Kutta scheme. To ensure the approximate equal total time consuming of the two methods, the time step ($\Delta t = 0.02$) is used for the loosely coupled method. The comparison of mode 1 response of the two methods is shown on the right hand of Fig. 3. The loosely coupled method has significantly enhanced the growth ratio of the oscillation. Based on the influence study of time-step sizes, it indicates the corresponding results can be obtained only for much small time-step. Namely, the present full implicit coupling method has higher compuational efficiency under the same requirements of accuracy and time cost.

Second Computational Test Case $M_\infty = 1.141$

Based on the baseline grid and the size of time step $\Delta t = 0.05$, computed dynamic responses are given in Fig. 4 for two dynamic pressures $q/q_e = 1.5$ and 1.8, respectively, at a supersonic Mach number $M_\infty = 1.141$, where $q_e = 105.3$ lbf/ft^2. For this Mach number, it has proved much more challenging to reproduce the reported experimental flutter behavier [2-4] due to the presence of the shock and corresponding shock/boundary layer interaction.

Through the average of the values for the last positive and nagative peaks, the amplification factors and response frequencies are obtained, which are $AF = 1.023$, $\omega = 122.62$ rad/sec and $AF = 1.172$, $\omega = 138.27$ rad/sec for the dynamic pressures $q/q_e = 1.5$ and 1.8, respectively, then the dynamic pressure and response frequency at the flutter point can be interpolated linearly. Table 3 summarizes the comparison of the present method with experimental data and other computations [2-4]. The present prediction overpredicts the flutter point like other computations, but the present method predicts a closer flutter point than that of other computations. To investigate the possible sources for the difference between the experiment and computation, Melville et al [4] examined the effects of various computational parameters, using 14 modes in structural model, using a third-order, upwind-based Roe schemes and changing the location of the computational transition location downstream from the leading edge to the 30% chord location. But only minimal effects of these changes were observed in the flutter response, it is not significant enough to explain the discrepancies between the computations and experiment. So their conclusion is that the actual physical conditions in the experiment may not be properly reflected in the computations. Significant changes in flutter speed and frequency could originate in a small difference in Mach numbers in the supersonic

flow region. Therefore, any small experimental error in Mach number could lead to significant differences between computed and experimental flutter properties.

Using the method aforementioned, the flutter boundary and frequency are calculated and compared with the experimental data over subsonic 0.338 to supersonic Mach numbers 1.141 in Fig. 5. The calculated results agree very well the experimental data in the subsonic and transonic range, but are higher than experimental values in the supersonic range.

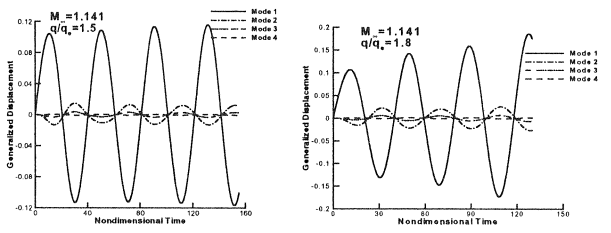

Fig. 4 Dynamic response of first four modes at $M_\infty = 1.141$, $q/q_e = 1.5$ and $q/q_e = 1.8$

Table 3 Summary of Flutter point predictions, $M_\infty = 1.141$

Method	q/q_e	$U_f/(b_s\omega_\alpha\sqrt{\mu})$	ω/ω_α
Present	1.454	0.492	0.515
Experiment	1.0	0.403	0.459
Reference 2	2.10	0.574	0.597
Reference 3	1.61	0.506	0.521
Reference 4	1.72	0.534	0.598

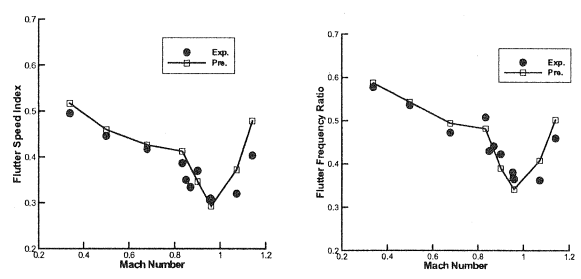

Fig. 5 Flutter speed and frequency for the AGARD 445.6 wing.

6. Concluding Remarks

A full implicit finite volume aeroelastic solver has been developed for transonic flutter simulation through the coupled subiteration of the Navier-Stokes equations and structural equations of motion. Results are presented for the AGARD 445.6 standard aeroelastic wing configuration over subsonic to supersonic Mach number range.

For the subsonic and transonic Mach number range, predictions of the flutter point agree very well with experimental data. The computation also shows the efficiency of the present method is higher than that of loosely coupled algorithm.

For the supersonic Mach number, due to the presence of the shock and the corresponding shock/boundary-layer interaction, the present calculation overpredicts the experimental flutter point, but the computed results are better than those of the previous computational results.

References

[1] G. P. Guruswamy: Vortical Flow Computations on Swept Flexible Wings Using Navier-Stokes Equations, *AIAA Journal,* Vo. 28, 1990, pp.2077-2084.

[2] S. A. Vermeersch, R. A. Weed, L. N. Sankar and P. Raj: Towards Cost-Effective Aeroelastic Analysis on Advanced Parallel Computing Systems, *AIAA Paper 97-0646,* Jan. 1997.

[3] E. M. Lee-Rausch and J. T. Batina: Wing Flutter Computations Using an Aeroelastic Model Based on the Navier-Stokes, *J. of Aircraft*, Vol.33 1996, pp.1139-1147.

[4] R. E. Gordiner and R. B. Melville: Transonic Flutter Simulations Using an Implicit Aeroelastic Solver, *J. of Aircraft*, Vol.37, 2000, pp.872-879.

[5] S. Obayashi and G. P. Guruswamy: Convergence Acceleration of a Navier-Stokes Solver for Efficient Static Aeroelastic Computations, *AIAA Journal*, Vol.33, 1995, pp.1134-1141.

[6] E. C. Jr. Yates: AGARD Standard Aeroelastic Configurations for Dynamic Response I-Wing 445.6, *AGARD-R-765,* 1988.

[7] B. S. Baldwin and H. L. Lomax: Thin Layer Approximation and Algebraic Model for Separated Turbulent Flows, *AIAA Paper 78-257,* 1978.

[8] S. Yoon and A. Jameson: Lower-Upper Symmetric –Gauss-Seidel Method for the Euler and Navier-Stokes Equations, *AIAA Journal Vol. 26,* 1988, pp. 1025-1026.

[9] R. B. Melville, S. A. Morton and D. P. Rizzetta: Implementation of a Fully-Implicit, Aeroelastic Navier-Stokes Solver, *AIAA paper 97-2039*, 1997.